Science Advances

AAAS

advances.sciencemag.org/cgi/content/full/2/8/e1600162/DC1

Supplementary Materials for

Experimental test of nonlocal causality

Martin Ringbauer, Christina Giarmatzi, Rafael Chaves, Fabio Costa, Andrew G. White, Alessandro Fedrizzi

Published 10 August 2016, *Sci. Adv.* **2**, e1600162 (2016)
DOI: 10.1126/sciadv.1600162

This PDF file includes:

- Relaxation of local causality
- Theoretical analysis of experimental imperfections
- Testing the new inequality
- Error analysis
- fig. S1. Efficiency η and visibility *v* requirements for a violation of inequality (*5*) in the main text without fair-sampling assumption.
- fig. S2. Measurement angles for inequality (*5*) in the main text.
- fig. S3. Distribution of statistical noise due to Poissonian counting statistics.
- table S1. Wave plate characterization data.
- References (*49–54*)

Here we discuss in detail the relation of the average causal effect to the CHSH violation. We also present the derivation of our novel 3-setting inequality and discuss data and error analysis.

Relaxation of local causality

In the following we will consider in detail the causal models that satisfy causal parameter independence, but may violate causal outcome independence. We will discuss explicitly the model in which A can influence B, keeping in mind that we also allow probabilities in which Alice's and Bob's roles are swapped (and convex combinations of the two). The corresponding probability distribution an be decomposed as

$$p(a,b\,|\,x,y)=\sum_{\lambda} p(a\,|\,x,\lambda)\,p(b\,|\,a,y,\lambda)\,p(\lambda) \tag{S1}$$

To understand how such a model allows for the generation of nonlocal correlations, consider the two following deterministic strategies

$$\begin{aligned}&\text{strategy 1}\ \rightarrow a=x,\ b=a(y\oplus 1)\\ &\text{strategy 2}\ \rightarrow\ a=x\oplus 1,\ b=y(a\oplus 1)\oplus a\end{aligned} \tag{S2}$$

Mixing the two strategies with equal probabilities generates the so-called Popescu-Rohrlich (*49*) distribution, $p(a,b\,|\,x,y)=(1/2)\delta_{a\oplus b,xy}$, which achieves maximal algebraic violation of the CHSH inequality, $S_2 = 4$. Crucially, however, despite the direct causal link from *A* to *B*, the above example does not permit to send signals between Alice and Bob at the level of empirical observations, satisfying $p(b|x, y) = p(b|x', y)$. In this case, however, signal locality does not follow from the causal structure in Fig. 1B), but rather from the precise choice of mixing probabilities in the above strategy. This kind of *fine-tuning* of model parameters in order to ensure no-signalling has been found to be a common feature of all causal explanations of Bell correlations (*12*).

The concept of fine-tuning plays an important role in causal discovery, which traditionally excludes fine-tuned models as unfaithful representations. The main justification for this step stems from the fact that assuming a uniform prior over the space of probabilistic parameters, the volume of it reproducing conditional independence relations not implied by the causal structure itself has measure zero (*15, 50*). In practice, however, estimation error issues due to data of finite sample size can result in the volume of unfaithful parameters being considerably large (*50*). From a purely causal inference perspective, this practical aspect—together with the fact that no faithful causal model can reproduce nonlocal correlations (*12*)—indicates that in order to conclusively eliminate fine-tuned models as a possible causal explanation to nonlocality, new methods are required.

As in the usual Bell scenario shown in Fig. 1A, each of the probabilities appearing in eq. (S1) can be identified with a deterministic function. To see that, consider the general case where Alice has m_x inputs and o_a outputs, that is, $x=0,\ldots,m_x-1$ and $a=0,\ldots,o_a-1$ (and analogously for Bob). The causal structure in Fig. 1B assures that $a = f_A(x, \lambda)$ which resembles the usual LHV model and therefore implies $o_a^{m_x}$ different deterministic functions f_A. For *b*, however, we have that $b = f_B(a,y,\lambda)$ requiring $o_b^{o_a m_y}$ different deterministic functions f_B. That is, in order to fully describe the causal structure we need an underlying hidden variable with $n=o_a^{m_x}o_b^{o_a m_y}$ possible values. In terms of these deterministic functions, the decomposition in (S1) can be rewritten as

$$p(a,b\,|\,x,y)=\sum_{\lambda}\delta_{a,f_A(x,\lambda)}\delta_{b,f_B(a,y,\lambda)}\,p(\lambda) \tag{S3}$$

It is useful to represent $p(a, b|x, y)$ as a vector $\mathbf{p}$ with components $\mathbf{p_j}$ labeled by the multi- index $j = (a, b, x, y)$. Similarly, the distribution of Λ can be represented by a vector with components $\mathbf{q}_\lambda = \mathbf{p}(\Lambda = \lambda)$. It follows then that $\mathbf{p} = T\,\mathbf{q}$ where T is a matrix with elements $T_{j,l} = \delta_{a,f_A(x,l)}\delta_{b,f_B(a,y,l)}$.

Analytical derivation of the relation between average causal effect $\mathrm{ACE}_{A\to B}$ and CHSH parameter S

We now show analytically that the experimentally accessible *average causal effect* is a suitable measure of causal influence in the CHSH scenario.

In general the measure

$$C_{A\to B}=\sup_{b,y,a,a'}\sum_{\lambda}p(\lambda)\left|p\left(b\,|\,\mathrm{do}(a),y,\lambda\right)-p\left(b\,|\,\mathrm{do}(a'),y,\lambda\right)\right| \tag{S4}$$

which quantifies the maximal shift (averaged over the unobservable variable Λ) in the probability of B caused by interventions in A, can be used to quantify the strength of the causal link from A to B. Indeed, it was shown in Ref. (*11*) that $\boldsymbol{C}_{A\to B}$ directly quantifies the degree of violation of causal outcome independence required for a causal explanation of the observed CHSH-violation as $\boldsymbol{C}_{A\to B} \geq \max[0, (S_2 - 2)/2]$, where the maximum is taken over all eight symmetries of the CHSH quantity under relabeling of inputs, outputs, and parties (34). The quantity $\boldsymbol{C}_{A\to B}$, however, is not directly experimentally accessible, therefore precluding its use in an experimental test of such a causal link.

Here we use an experimentally accessible variant of $\boldsymbol{C}_{A\to B}$, which does not require knowledge of the hidden variable, the *average causal effect*

$$\begin{aligned}\mathrm{ACE}_{A\to B}&=\sup_{b,y,a,a'}\left|p(b\,|\,\mathrm{do}(a),y)-p(b\,|\,\mathrm{do}(a'),y)\right|\\&=\sup_{b,y,a,a'}\pm\left(p(b\,|\,\mathrm{do}(a),y)-p(b\,|\,\mathrm{do}(a'),y)\right)\end{aligned} \tag{S5}$$

This expression quantifies the average causal effect from variable A into variable B. That is, the least shift in the probability distribution of B that must be observed upon intervention on the variable A, if indeed the underlying causal structure is that shown in Fig. 1B in the main text. We are therefore interested in the following optimization problem

$$\begin{aligned}\underset{\mathbf{q}\in R^n}{\text{minimize}}\quad&\mathrm{ACE}_{A\to B}\\\text{subject to}\quad&T\mathbf{q}=\mathbf{p}\\&\left\langle\mathbf{1}_n,\,\mathbf{q}\right\rangle=1\\&\mathbf{q}\geq\mathbf{0}_n\end{aligned} \tag{S6}$$

The two last constraints follow from the fact that the hidden variable Λ should be described by a well defined probability distribution (positive and normalized).

To write the optimization problem eq. (S6) as a standard linear program, notice that

$$p(b\,|\,\mathrm{do}(a), y) - p(b\,|\,\mathrm{do}(a'), y) \tag{S7}$$

$$= \sum_{\lambda} p(\lambda)(\delta_{b, f_B(a,y,\lambda)} - \delta_{b, f_B(a',y,\lambda)}) \tag{S8}$$

$$= \sum_{i} q_i v_i = \langle \mathbf{v}, \mathbf{q} \rangle \tag{S9}$$

where the vector $\mathbf{v} = \mathbf{v}(a, a', y, b)$ fully characterizes the action of the Kronecker-symbols in Eq. (S8). The ACE measure (S5) can then be recast as

$$\mathrm{ACE}_{A\to B} = \max_{i=1,\ldots,2L} \langle \mathbf{q}, \mathbf{v}_i \rangle = C\mathbf{q} \tag{S10}$$

Here, the index i parametrizes the $2L$ possible instances of (a, a', y, b) with $x \neq x'$ (the factor 2 coming from the ± signs in Eq. (S5)) and $\mathbf{v}_i = v(a,a',y,b)$ denotes the vector corresponding to that instance. The matrix C subsumes all these different instances, that is, $C \coloneqq \sum_{i=1}^{L} |\mathbf{e}_i\rangle\langle \mathbf{v}_i|$ where $\mathbf{e}_i$ stands for an orthonormal basis.

The optimization problem in eq. (S6) is then equivalent to a standard linear program

$$\begin{aligned} \underset{\mathbf{v},\mathbf{q}}{\text{minimize}} \quad & v \\ \text{subject to} \quad & T\mathbf{q} = \mathbf{p} \\ & \langle \mathbf{1}_n, \mathbf{q} \rangle = 1 \\ & \mathbf{q} \geq \mathbf{0}_n \\ & C\mathbf{q} \leq v\ . \end{aligned} \tag{S11}$$

As proved in Ref. (*11*), to obtain the solution of this problem for any vector **p** encoding the full probability distribution p(a,b|x,y), we have to consider the dual optimization problem. In practice, that means that solving eq. (S11) is equivalent to evaluating

$$\max_{1\leq i\leq K} \langle \mathbf{d}_i, \mathbf{p} \rangle$$

where $\{\mathbf{d}_i\}_{i=1}^{K}$ denotes the vertices of the dual feasible region (see Ref. (*11*) for further details).

We have performed such an analysis for the particular case of the CHSH scenario ($m_x=m_y=o_a=o_b=2$) using PORTA (51), a standard software for the evaluation of extremal points of a polyhedron. Similarly to what happens to the measure $C_{A\to B}$ (see Supplemental material of Ref. (*11*)), the extremal points of the dual region correspond to non-signaling constraints and all the symmetries of the CHSH inequality (up to a constant factor), implying that

$$\mathrm{ACE}_{A\to B} \geq \max[0,(S-2)/2] \tag{S12}$$

Proving the new inequality

As shown above, a relaxation of causal outcome independence, while maintaining causal parameter independence, allows for the classical explanation of any nonlocal correlations in the CHSH scenario, where the two parties perform two possible dichotomic measurements. However, if the parties perform three or more measurements each, this does not hold anymore.

The decomposition (S3) defines a polytope of correlations that are compatible with the causal model in Fig. 1B in the main text. This polytope is characterized by $n = o_a^{m_x} o_b^{o_a m_y}$ extremal points. Therefore, for a fixed number of measurements and outcomes, one can resort to usual convex optimization software in order to find its description in terms of finitely many Bell inequalities. As shown in Ref. (11), one of the Bell inequalities characterizing the polytope in the case $o_a = o_b = 2$ and $m_x = m_y = 3$ is given by the inequality

$$S_3 = \langle E_{00}\rangle - \langle E_{02}\rangle - \langle E_{11}\rangle + \langle E_{12}\rangle - \langle E_{20}\rangle + \langle E_{21}\rangle \leq 4 \tag{S13}$$

An easy way of proving that this inequality in fact holds is to verify that for each of the $n = 2^3 2^6$ extremal points defining the polytope this inequality is satisfied.

A similar argument can be used to prove that this inequality is also valid if we reverse the roles of Alice and Bob. That is, in this case we allow the outcomes of Alice to depend on the outcomes of Bob

$$p(a,b\,|\,x,y) = \sum_{\lambda} p(a\,|\,x,b,\lambda)\, p(b\,|\,y,\lambda)\, p(\lambda) \tag{S14}$$

Since both the models eq. (S1) and eq. (S14) respect inequality (S13), so does a convex combination of both of them. In other words, any model of the form

$$\begin{aligned} p(a,b\,|\,x,y) = &\sum_{\lambda} p(a\,|\,x,\lambda)\, p(b\,|\,y,a,\lambda)\, p(\lambda) + \\ &\sum_{\mu} p(a\,|\,x,b,\mu)\, p(b\,|\,y,\mu)\, p(\mu) \end{aligned} \tag{S15}$$

with $\sum_{\mu} p(\mu)+\sum_{\lambda} p(\lambda)=1$, respects inequality (*5*). Any pure two-qubit entangled state, however, can generate correlations violating this inequality (*11*). This allows us to show unambiguously and based on observational data only, that a direct causal influence from one outcome to the other cannot explain quantum correlations.

Theoretical analysis of experimental imperfections

Any experiment suffers from imperfections in the form of detector inefficiencies, noise and other possible forms of loss. Practically our experiment thus relies on a fair-sampling assumption. Here we provide a short analysis of the requirements for avoiding this assumption in tests of inequality (*5*). Our analysis is similar to what is usually done for Bell inequalities, for example, the CHSH inequality (*52*, *53*).

To describe the inefficiency of the photon detectors, we model the projective measurements being performed in the experiment via the following POVM with elements (*54*)

$$\begin{aligned} M_{\uparrow} &= \eta_{\uparrow}\left|\uparrow\right\rangle_s\left\langle\uparrow\right| + (1-\eta_{\downarrow})\left|\downarrow\right\rangle_s\left\langle\downarrow\right| \\ M_{\uparrow} &= \eta_{\downarrow}\left|\downarrow\right\rangle_s\left\langle\downarrow\right| + (1-\eta_{\uparrow})\left|\uparrow\right\rangle_s\left\langle\uparrow\right| \end{aligned} \qquad \text{(S16)}$$

For perfect efficiencies $\eta_{\uparrow}=\eta_{\downarrow}=1$ this POVM implements a projective measurement along the direction defined by *s*, that is, $\left|\uparrow\right\rangle_s, \left|\downarrow\right\rangle_s$ are eigenstates of the observable $\left|\uparrow\right\rangle_s\left\langle\uparrow\right| - \left|\downarrow\right\rangle_s\left\langle\downarrow\right|$. Following the usual treatment of detection inefficiencies (*52*-*54*), given a non-click event of the detectors happening with probability η (assumed to be the same for both detectors), we bin it together with the $\downarrow$-outcome. That is, our faulty measurements are described by eq. (S16) with $\eta_{\downarrow}=1$ and $\eta_{\uparrow}=\eta$.

We also consider errors in the preparation of the states. To that aim we consider the initial two-qubit state to be affected by white noise (parameterized by the visibility v)

$$\rho_{\gamma}(v) = v\left|\Psi_{\gamma}\right\rangle\left\langle\Psi_{\gamma}\right| + (1-v)\mathbf{1}/4\,, \qquad \text{(S17)}$$

where $\Psi_{\gamma}=\cos\gamma\left|HV\right\rangle+\sin\gamma\left|VH\right\rangle$ represents the pure two-qubit entangled state that we would ideally prepare.

For different values of γ we have performed a numerical optimization over all possible POVMs eq. (S16) in order to find the minimum values of v and η leading to the violation of Inequality (*5*) without requiring the fair-sampling assumption. The results are shown in fig. S1. As can be seen, the smaller is the initial entanglement (parameterized by the angle θ) the less robust is the violation of the inequality as function of the visibility and detector inefficiency. For a maximally entangled state the minimum required visibility and efficiency are, respectively, $v_{\text{crit}} \sim 0.77$ and $\eta_{\text{crit}} \sim 0.88$. For comparison, we also compute the requirements for the usual CHSH inequality

(*52*, *53*). Not surprisingly, since our inequality excludes a larger class of causal models, it has more stringent experimental requirements.

Theoretical analysis of experimental imperfections

Similarly to the standard CHSH inequality, our 3-setting inequality (5) in the main text can be tested using only measurements in the equatorial plane of the form $O = \cos(\theta)Z + \sin(\theta)X$. Numerical results suggest that this is indeed optimal and the maximal violation of the inequality is achieved for $\theta_0^{(A)} = -\pi/6, \theta_1^{(A)} = 7\pi/6, \theta_2^{(A)} = \pi/2, \theta_0^{(B)} = -\pi/3, \theta_1^{(B)} = \pi/3, \theta_2^{(B)} = \pi$, where the superscript denotes the party and the subscript denotes the number of the measurement. Using these measurement settings we obtain

$$S_3 = \frac{3}{2}\sqrt{3}(1+\sin(2\gamma))$$

Note that since the concurrence $C = |\sin 2g|$ this corresponds to a linear relationship between S_3 and the concurrence of the used state.

As pointed out in the main text, inequality (*5*) can indeed be violated by every entangled quantum state. This is clearly demonstrated by $\theta_0^{(A)} = -\alpha, \theta_1^{(A)} = \alpha + \pi, \theta_2^{(A)} = \pi/2, \theta_0^{(B)} = -\beta, \theta_1^{(B)} = \beta, \theta_2^{(B)} = \pi$, where the optimal angles a, b can be found analytically as a function of the state parameter g. In this case we obtain:

$$S_3 = \left(\frac{\sqrt{\cos(4\gamma)+7} - \sqrt{2}(\cos(2\gamma)-3)}{2\cos^2(\gamma)} \right) \left(\sqrt{\cos(2\gamma) + \sqrt{2}\sqrt{\cos(4\gamma)+7} - 3} \right)$$

The corresponding angles a and b are shown in fig. S2.

Error analysis

Here we discuss the details of the error analysis for both experiments introduced in the main text.

Any photonic experiment suffers from statistical noise due to the Poissonian nature of the single-photon source and detection. Additionally it is a common feature for experiments measuring bounded quantities (such as $\mathrm{ACE}_{A\to B}$) that observed distributions feature significant asymmetry close to the boundaries, making the observation of extreme values very unlikely. To illustrate this effect, fig. S3 shows simulated statistics for $\mathrm{ACE}_{A\to B}$ assuming perfect measurement and only Poissonian noise at a total number of 48000 single-photon events. For our choice of quantum states, the distribution of single-photon clicks is such, that higher entangled states are more susceptible to this form of noise. As a consequence, the median of the distribution increases with

entanglement from 0.0048 to 0.0068, with 3σ confidence intervals of [0.0002, 0.0155] and [0.0003, 0.0219], respectively. Note that all 3σ-intervals quoted here and in the main text correspond to the intervals that contain ~99.73% of the data (in analogy with the 3σ-region for a normal distribution) and are thus asymmetric around the median of the distribution, see fig. S3.

Besides the statistical errors there are various sources of systematic errors, which explain the consistent offset of the measured $\mathrm{ACE}_{A\to B}$ from 0. For the interventionist experiment it is crucial that all CHSH measurements are performed in the equatorial plane, while the intervention acts on the poles of the Bloch sphere. The relevant waveplates are one HWP each to set Alice' and Bob's measurement basis, and one QWP for the intervention. The relative phase-shifts imparted by these waveplates and their accuracy are listed in table S1. These errors result in a tilt of the intervention from the orthogonal orientation of $0.0109^{+0.0122}_{-0.0009}$ and Alice's and Bob's measurement planes are tilted by $0.1403^{+0.0004}_{-0.0005}$, and $0.050^{+0.013}_{-0.010}$, respectively.

The accuracy of the intervention polarizer is $\Delta\phi = 0.14^{\circ}$, with a contrast better than 7000:1. Alice's and Bob's measurement PBS have a contrast of greater than 500:1 and 8000:1, respectively and are aligned to each other to a contrast of 1000:1. These systematic imperfections were taken into account in a Monte Carlo simulation, and resulted in a slight increase in the offset of the median from zero and the variance of the expected statistical distribution obtained from simulating Poissonian noise. This suggests that the in Fig. 3 in the main text is consistent with 0, when taking into account systematic imperfections and statistical noise.

Figures and Tables

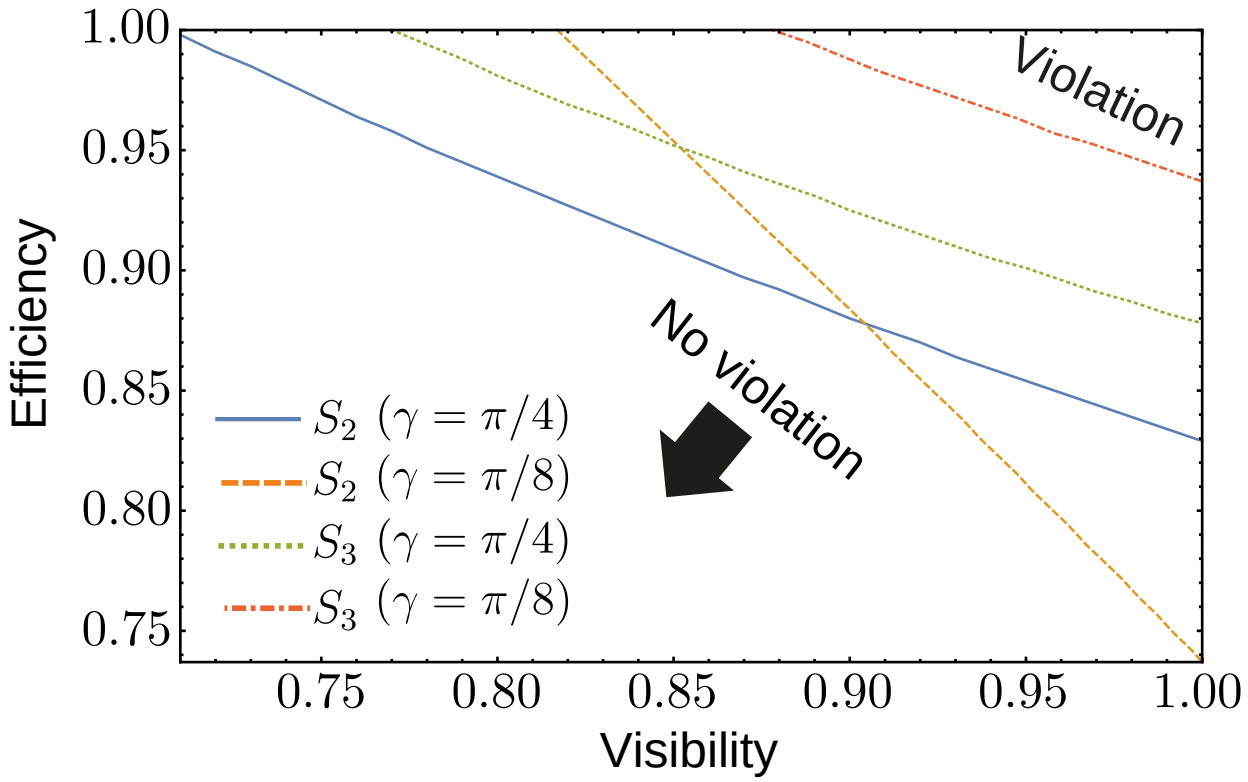

fig. S1. Efficiency η and visibility *v* requirements for a violation of inequality (*5*) in the main text without fair-sampling assumption. For a maximally entangled state ($g = p/4$) inequality (*5*) of the main text is violated above the green, dashed line, while the CHSH inequality is violated above the blue, solid line. For a non-maximally entangled state ($g = p/8$) the corresponding lines are red dot-dashed for inequality (*5*) of the main text and orange, dashed for CHSH.

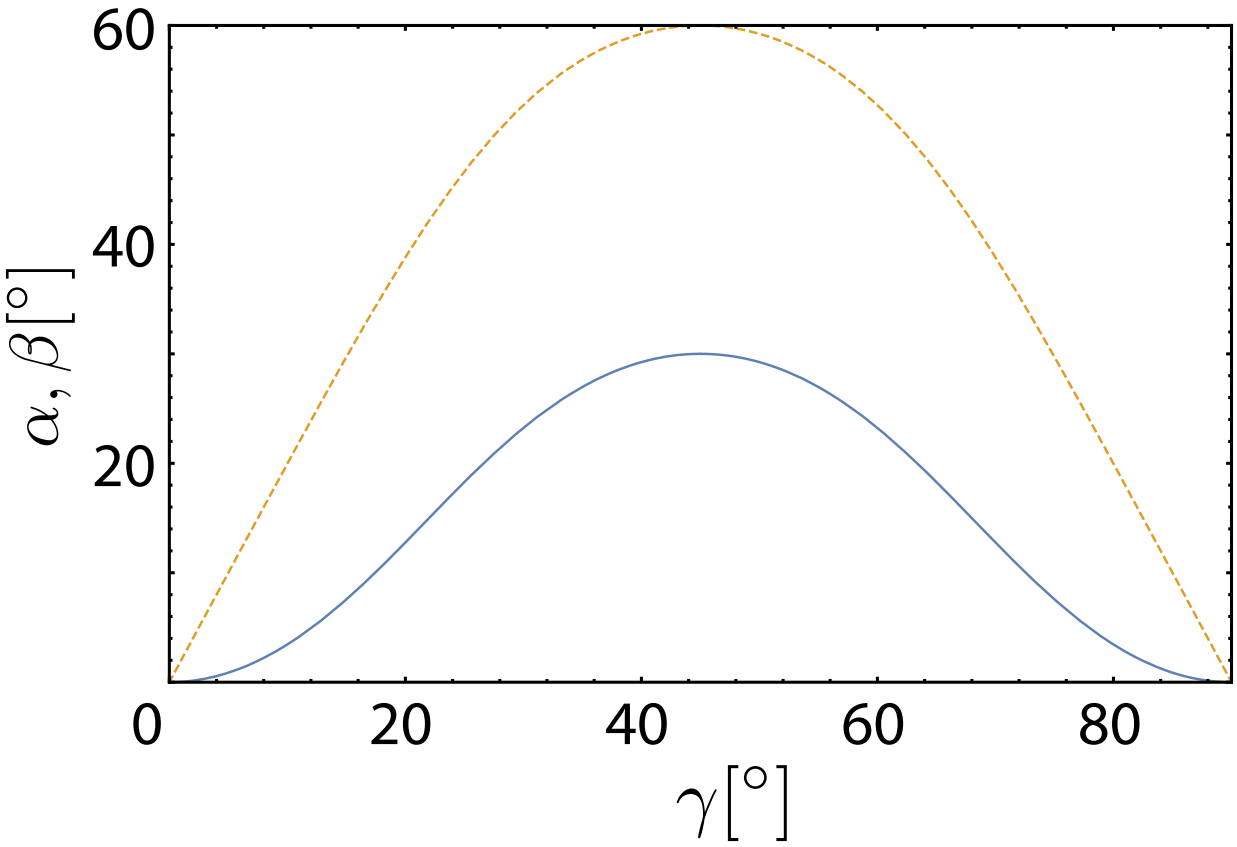

fig. S2. Measurement angles for inequality (5) in the main text. Alice's measurement angle α shown in solid, blue, and Bob's measurement angle β in dashed, orange.

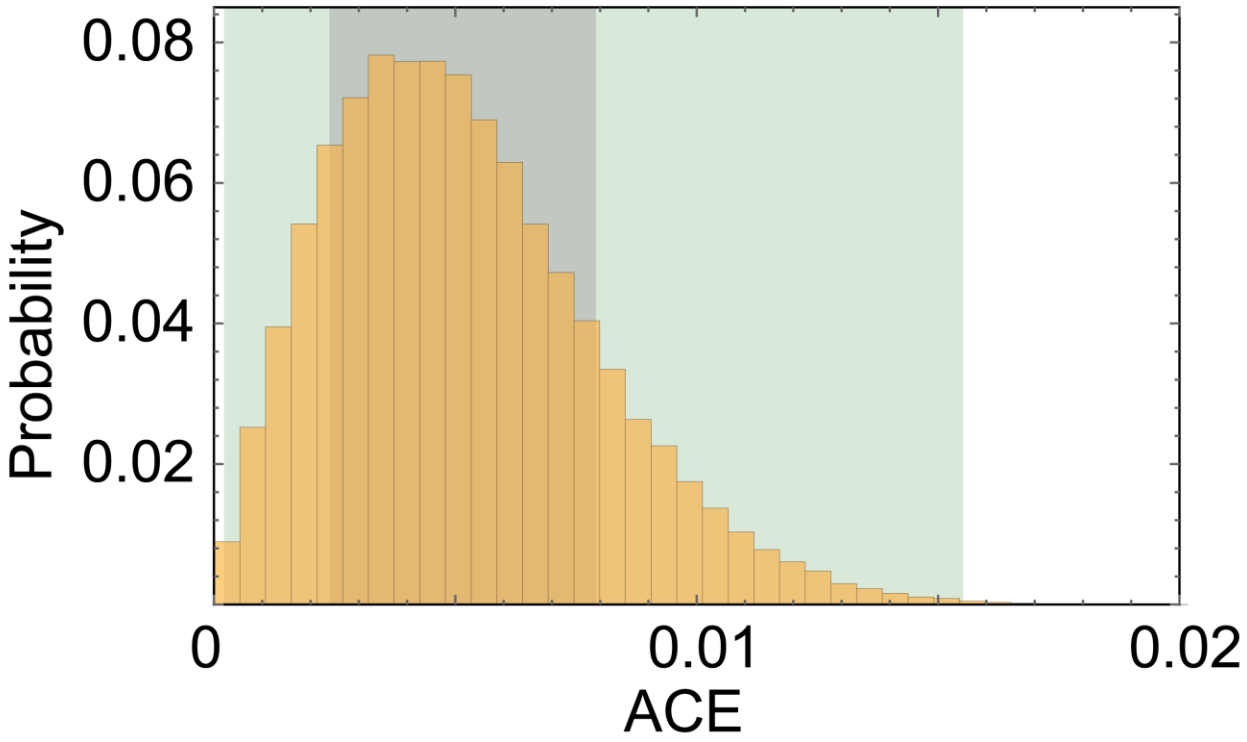

fig. S3. Distribution of statistical noise due to Poisson counting statistics. The dark, purple shaded area corresponds to the ~68.27% (1σ) confidence interval, while the light, green area is the ~99.73% (3σ) interval. These have been chosen for comparability with normal distributed data. Data was obtained from 100,000 runs of a Monte-Carlo simulation of the Poisson counting statistics for perfect measurements.

table S1. Waveplate characterization data. Shown are the standard deviations Δf in the angles of the optical axes as determined from fits to the measured coincidence counts, as well as the retardance r (in measures of λ/2) obtained from the visibility of the fringes observed in the same data, for the relevant waveplates.

Element	Δf(°)	r
HWP (X)	0.04	0.955
HWP (Y)	0.04	0.978
QWP (I)	0.13	0.503